



HAL
open science

Electron acceleration and small-scale coherent structure formation by an Alfvén wave propagating in coronal interplume region

K. Daifallah, Fabrice Mottez

► **To cite this version:**

K. Daifallah, Fabrice Mottez. Electron acceleration and small-scale coherent structure formation by an Alfvén wave propagating in coronal interplume region. *Astronomical Notes / Astronomische Nachrichten*, 2017, 338 (7), pp.781-789. 10.1002/asna.201713364 . hal-02392030

HAL Id: hal-02392030

<https://hal.science/hal-02392030>

Submitted on 3 Dec 2019

HAL is a multi-disciplinary open access archive for the deposit and dissemination of scientific research documents, whether they are published or not. The documents may come from teaching and research institutions in France or abroad, or from public or private research centers.

L'archive ouverte pluridisciplinaire **HAL**, est destinée au dépôt et à la diffusion de documents scientifiques de niveau recherche, publiés ou non, émanant des établissements d'enseignement et de recherche français ou étrangers, des laboratoires publics ou privés.

Electron acceleration and small scale coherent structures formation by an Alfvén wave propagating in coronal interplume region

K. Daïffallah^{1,*} and F. Mottez²

¹ Observatory of Algiers, CRAAG, Route de l'Observatoire, BP 63, Bouzaréah 16340, Algiers, Algeria

² Laboratoire Univers et Théorie, CNRS, Observatoire de Paris, Université Paris Diderot, PSL Research university, Meudon, France

Received XXXX, accepted XXXX

Published online XXXX

Key words Sun: corona – (Sun:) solar wind – acceleration of particles – instabilities – plasmas – waves

We use 2.5-D electromagnetic particle-in-cell simulation code to investigate the acceleration of electrons in solar coronal holes through the interaction of Alfvén waves with an interplume region. The interplume is modeled by a cavity density gradients that are perpendicular to the background magnetic field. The aim is to contribute to explain the observation of suprathermal electrons under relatively quiet sun. Simulations show that Alfvén waves in interaction with the interplume region gives rise to a strong local electric field that accelerates electrons in the direction parallel to the background magnetic field. Suprathermal electron beams and small-scale coherent structures are observed within interplume of strong density gradients. These features result from non linear evolution of the electron beam plasma instability.

Copyright line will be provided by the publisher

1 Introduction

The origin of solar wind suprathermal electrons remains an unsolved problem in solar physics. Different acceleration processes based on magnetic reconnection have been proposed. However, observations indicate that electrons are accelerated even under quiet solar conditions (Lin, 1980). Pierrard et al. (1999) found from the observational data of the *WIND* spacecraft at 1 A.U that suprathermal particles can be originated from low altitude corona.

In this work, we look at a process which takes place in a small area in the solar corona where parallel electric fields to the background magnetic field can accelerate electrons efficiently. The origin of these parallel electric fields can be associated with regions of depletion of density, i.e., plasma cavities

The possible link of the acceleration regions with plasma cavities can be seen for instance in the Earth auroral zone. Density cavities with a small width (a few km) were observed in this region by space probes like *Viking*, *Freja* and *FAST* at altitudes between 2000 and 12.000 km (Hilgers et al. 1992; Louarn et al. 1994; Carlson et al. 1998). In the Earth auroral zones, where in-situ measurement were done, the plasma cavities are systematically related to the presence of electron beams and strong electrostatic fields. It was shown that the propagation of Alfvén waves along an inhomogeneous plasma in Earth magnetosphere with perpendicular density gradients can efficiently accelerate electrons to a few keV (Génot, Mottez & Louarn 2001; Génot, Louarn & Mottez 2004; Mottez & Génot 2011).

In this study, we expect another source of suprathermal electrons different from solar flares, namely the interplume region in the polar coronal holes, where the solar wind escapes with a high-speed.

Plumes are prominent bright and narrow structures of the solar corona, observable both in visible and ultraviolet (UV). They are associated to open magnetic field lines which expand from the chromospheres to the upper corona. Interplumes appear as darker and sharper regions surrounding the bright plumes (Wilhelm 2006; Wilhelm et al. 2011; Poletto et al. 2015).

Observations show that in the low corona, the density in plumes can be four to seven times more than in interplume regions. However, with increasing height, this density decreases faster than those of interplumes and the density ratio becomes smaller (see Figure 17 in Wilhelm et al. 2011). The electron densities in plume is estimated to be up to about 10^9 cm^{-3} for $R > R_{\odot}$ (Wilhelm et al. 2011). The observed density of a typical plume with cylindrical symmetry has a radial gradient profile which declines with the distance from the plume axis (Newkirk & Harvey 1968). Given that, the density in the interplume region will show a cavity-like profile.

Using the Solar Optical Telescope aboard *Hinode*, Tsuneta et al. (2008) found that the polar region shows a many vertically oriented magnetic flux tubes with field strengths as strong as 1 kG. These open magnetic fields are dominated by a single polarity (Ito et al. 2010). Tsuneta et al. (2008) estimate the average total magnetic flux for the polar regions situated at latitudes above 70° . They found values between 3.1 and 13.9 G. These numbers should be

* Corresponding author: k.daïffallah@craag.dz

regarded as minimum values. McIntosh et al. (2011) show that the observed densities and phase speeds associated to transverse oscillations in the coronal holes and quiet Sun regions are compatible with the presence of magnetic fields of the order of 10 G.

In general, the electron temperature in coronal holes is estimated to be between 0.7 and 2 MK at height $h = 0$ (see Figure 18 in Wilhelm et al. 2011).

Waves are present both in plumes and interplumes. Indirect observations of transverse Alfvén waves in coronal holes have been reported by many authors (see review by Banerjee et al. 2011). Using comparison between (*SDO/AIA*) data of the observed Alfvénic motions and synthetic data from Monte Carlo simulation, McIntosh et al. (2011) demonstrate that the wave energy flux is sufficient to accelerate the fast solar wind and heat the quiet corona. Transverse Alfvén waves have been detected directly for the first time in solar polar plumes by Thurgood et al. (2014) using observations from (*SDO/AIA*) instrument. However, their results indicate that Alfvén waves cannot be the dominant energy source for fast solar wind acceleration in coronal holes.

Wilhelm et al. (1998) measured velocities in coronal-holes plasma with the SUMER instrument on *SOHO*. They found strong accelerations of ions in interplume lanes in comparison to those observed in plume regions. Observations with *Hinode/EIS* and *SOHO/SUMER* by Gupta et al. (2010) show that interplumes support either Alfvénic or fast magneto-acoustic waves, while plumes support more the slow magneto-acoustic waves. Moreover, the authors observed for the first time a signature of acceleration of the waves in interplume regions. These observations provide strong indications that the propagation of Alfvén waves in interplume regions play a major role on the acceleration of the fast solar wind. This conclusion is in agreement with several earlier works (see Poletto et al. 2015). Alfvén waves propagate from lower solar atmosphere transporting energy to the corona along regions of open magnetic field, such as polar coronal holes. A fraction of this mechanical energy is converted to thermal energy which dissipates and heats coronal holes and accelerates the fast solar wind. Various MHD models based on turbulences and interaction of Alfvén waves with inhomogeneous plasmas were proposed to explain the dissipation mechanisms (see review by Ofman 2005).

Moreover, the non-linear turbulent evolution of the Alfvén wave activity can favour the transfer of energy from long wavelengths to shorter ones. We can therefore expect Alfvén waves in the MHD range of long wavelengths, as well as of shorter lengths whose frequencies scale as the ion gyro-frequency (Bale et al. 2005; Podesta & TenBarge 2012). This phenomenon is evidenced with in-situ measurements in the solar wind (Goldstein & Roberts 1999). Actually, shorter wavelengths have even been seen in space plasma, cascading down to electron scale lengths (Sahraoui et al. 2013). These observations have been supported by

EMHD numerical simulations (Biskamp et al. 1999), where the Alfvénic fluctuations can reach frequencies of the order of the ion gyrofrequency. These theoretical works show that the spectrum of Alfvén waves extended over a broad interval of frequencies/wavelengths is relevant for a large domain of plasma parameters and it can be expected in many areas of the solar environment, including the low beta regions of its corona (Zhao, Wu & Lu 2013).

This type of cascade gives rise to kinetic Alfvén waves when the perpendicular wavenumber $k_{\perp} \neq 0$. Beyond the first several solar radii of height from the solar surface, the plasma in coronal holes becomes collisionless, which makes it possible to use multi-fluid kinetic processes to treat the plasma. Then wave-particle kinetic interactions will act as effective collisions in this plasma, and may lead to heating, as discussed by several kinetic models (see review by Cranmer 2009).

In this context, Wu & Fang (2003) investigated the dissipation of a kinetic Alfvén waves through an empirical model of a plume and uniformly low- β magnetized coronal hole surrounding media. The dense plume is characterized by a radial steady flow with transverse pressure balance. The authors conclude that the dissipation of the kinetic Alfvén waves energy provide a sufficient local electron heating to balance the enhanced radiative losses of the bright plumes.

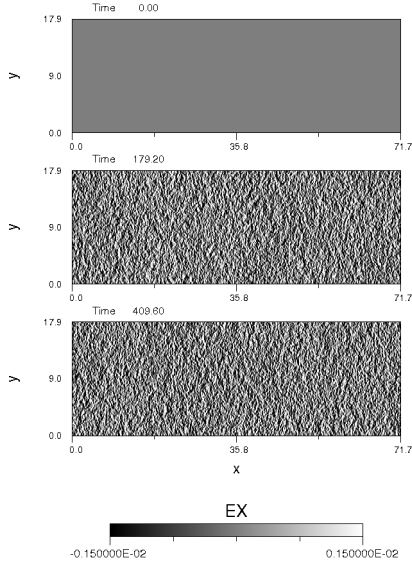
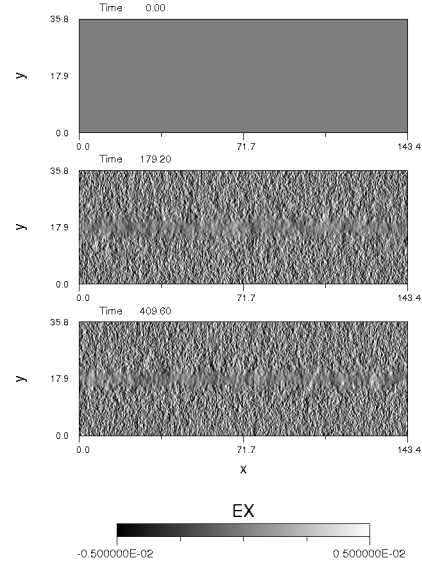
Tsiklauri (2011) simulated the propagation of inertial and kinetic Alfvén waves through inhomogeneous collisionless plasma that mimics solar coronal loops. This study considered plasma over-densities (instead of cavities). There was a production of energetic electrons that can be a cause of the X-ray emissions from the solar atmosphere. A recent study of parallel electron acceleration was conducted with 3D simulations (Tsiklauri 2012). The study considers a low beta plasma with left-hand polarized Alfvén waves of relatively high frequency $\omega = 0.3\omega_{ci}$ propagating over sharp density gradients. (It is important to notice that for a given wavelength, the left-hand polarized mode has a lower frequency than the right-hand polarized one, and that its frequency cannot be larger than ω_{ci}). This study confirms that when the gradients typical size is $\sim c/\omega_{pe}$, parallel electric fields develop. They cause parallel electron acceleration, and perpendicular ion heating. The author suggests that this process is at work in the solar flare acceleration regions.

In the present paper, we present Particle In Cell (PIC) numerical simulations of the interaction of Alfvén waves with an inhomogeneous plasma. The interplume structure is modeled by plasma with density gradients in the transverse direction to the background magnetic field. The plasma conditions are those expected in coronal hole region. Our main goal is to explain the observed suprathermal electrons which are originate from coronal holes and particularly from interplume regions. The mechanism that we describe can contribute to the heating and the acceleration of solar fast wind.

The simulation model and parameters are exposed in section 2. The global electric field structure and the electron acceleration are shown in sections 3 and 4 respectively.

Table 1 Simulations parameters in normalised units.

| Run | Particles per cell | Cavity depth p | B_0 | wavelength | $\delta B/B_0$ | V_{Te} | $(m_i/m_e)\beta$ |
|-----|--------------------|------------------|-------|------------|----------------|----------|------------------|
| A | 100 | No cavity | 0.315 | 71.7 | 0.3 | 0.07 | 0.05 |
| B | 100 | 1 | 0.315 | 143.4 | 0 | 0.14 | 0.19 |
| C | 400 | 0.75 | 0.315 | 71.7 | 0.3 | 0.07 | 0.05 |
| D | 400 | 1 | 0.315 | 143.4 | 0.1 | 0.14 | 0.19 |

**Fig. 1** Run A: snapshots from $t = 0$ to $t = 409.6$ of the parallel component of electric field $E_x(x, y)$.**Fig. 2** Run B: snapshots from $t = 0$ to $t = 409.6$ of the parallel component of electric field $E_x(x, y)$.

Small scale coherent structures and their link with beam instabilities are exposed in section 5. Then we conclude.

2 Simulation model and parameters

In the solar corona, the electron plasma frequency ω_{pe} is larger than the electron cyclotron frequency ω_{ce} . The ratio of the two frequencies is given by the equation

$$\frac{\omega_{pe}}{\omega_{ce}} \approx 3.2 \times 10^{-3} \frac{n_0^{1/2}}{B_0} \quad (1)$$

where the electron density n_0 is in cm^{-3} , and the magnetic field strength B_0 is in gauss (G).

In all the simulations, we assume a uniform background magnetic field B_0 in the parallel direction x , which is the solar radial direction. The strength of the magnetic field is set to be $B_0 = 10$ G. The background electron density is given by $n_0 = 10^8 \text{ cm}^{-3}$. The electronic temperature T_e is assumed to vary from 10^6 to 10^8 K, which corresponds to

$T_e = 2 \text{ keV}$ and $T_e = 10 \text{ keV}$ respectively (see Introduction for these plasma conditions).

When Alfvén waves propagate over a perpendicular density gradient with a typical scale length that is below the MHD limits, inertial and kinetic effects play a fundamental role in the creation of the parallel electric field. Their behaviour is then very dependent on the parameter $(m_i/m_e)\beta$, where β is the ratio of the kinetic pressure to the magnetic pressure. With the plasma characteristics given above, $(m_i/m_e)\beta \ll 1$. For instance, with $T \sim 2 \text{ keV}$, $B_0 = 10$ G and $n_0 = 10^8 \text{ cm}^{-3}$, and $\omega_{pe}/\omega_{ce} = 3.17$ (Equation 1), we find $(m_i/m_e)\beta = (v_{Te}/c)^2 (\omega_{pe}/\omega_{ce})^2 \sim 0.05$. We are in the so-called inertial regime described by Goertz (1984). For $B_0 = 10$ G, $n_0 = 10^8 \text{ cm}^{-3}$ and $T \sim 10 \text{ keV}$, we find $(m_i/m_e)\beta = 0.2$ still corresponds to the inertial regime. It is therefore important that the plasma regime in the numerical simulations also corresponds to $\omega_{pe}/\omega_{ce} > 1$ and $(m_i/m_e)\beta \ll 1$.

However, when the temperature goes up to 10^8 K we leave the inertial regime and reach the kinetic regime, but

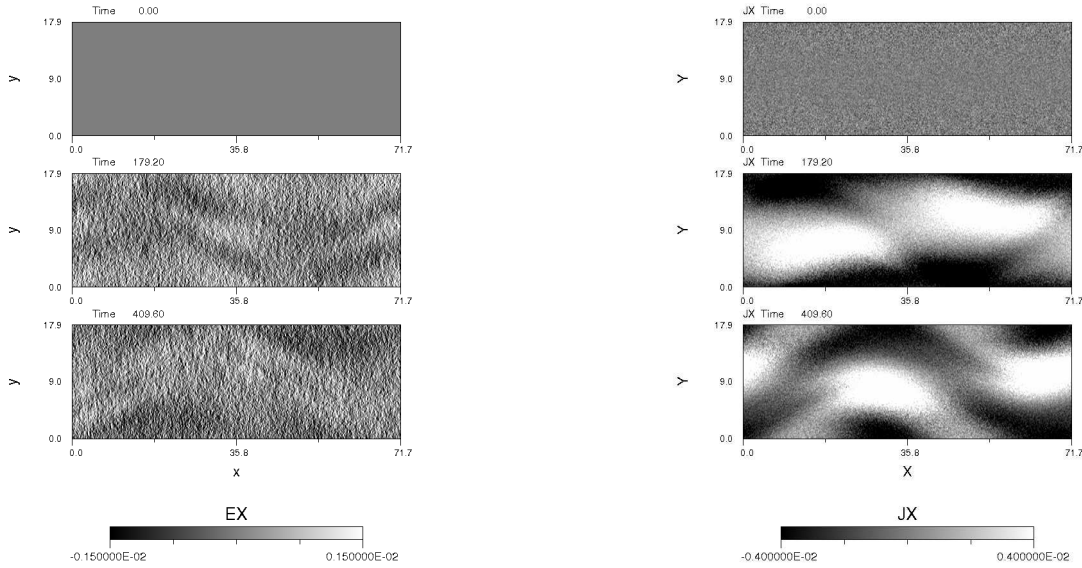


Fig. 3 Run C: snapshots from $t = 0$ to $t = 409.6$ of the parallel component of electric field $E_x(x, y)$ in left panel, and the parallel current density associated to the electrons $J_x(x, y)$ in right panel.

such temperatures are exceptional. The simulations presented in this paper are done in the inertial regime.

We use an electromagnetic PIC code developed in Mottez, Adam & Heron (1998) which takes into account the full electron and ion motion. The code is 2D in space ((x, y) coordinates) and 3D in fields and velocity components. The boundary conditions are periodic in x and y directions.

The physical variables used in the code are all dimensionless. The inverse of time and frequency are normalized to electron plasma frequency ω_{p0} which corresponds to the uniform background electron density n_0 . The velocities are normalized to the speed of light c . The reference units are the mass of the electron m_e for the masses, c/ω_{p0} for distances, ω_{p0}/c for the wave vectors, the electric charge e for charges, the electron density n_0 for charge densities, $c\omega_{ce}/\omega_{p0}$ for the electric field. In what follows, in the absence of specific mention, all the figures and numerical values are expressed in dimensionless units.

We present a series of four numerical simulations whose parameters are summarised in Table 1. The dimensionless background magnetic field B_0 is given by the frequency ratio ω_{ce}/ω_{pe} . For $B_0 = 10$ G and $n_0 = 10^8$ cm $^{-3}$, the dimensionless background magnetic field will be $B_0 = 0.315$ (Equation 1). The dimensionless thermal velocity V_{Te} is 0.07 or 0.14. The electron temperature T_e and the ion temperature T_i are equal. The simulation box size is $L_x \times L_y = 1024\Delta x \times 256\Delta y$ where the cell size $\Delta x = \Delta y = \lambda_{De} = V_{Te}$ is one Debye length. For economy of computational resources, the ion to electron mass ratio is reduced to $m_i/m_e =$

100. The simulations are run over 2048 or 4096 time steps of duration $\Delta t = 0.2$.

For the sake of simplification, we modelize a single interplume embedded between two plumes of identical density profile. This will give a cavity profile to the interplume density .

The interplume in Runs B, C and D is characterized by a plasma cavity of infinite length along the solar radial direction x with a Gaussian density profile in the transverse (y) direction

$$\frac{n(y)}{n_0} = 1 - p[\exp\{-Y^2/R^2\}] \quad (2)$$

where $n(y)$ is the density on the interplume, n_0 is the density on the surrounding plumes axis .

$Y = y - N_y/2$, where $N_y = 256$ is the number of cells in y direction and p is the depth of the cavity $n_{min}/n_0 = 1 - p$, and R is the half of the cavity width. In all of these simulations, we have set $R = N_y/2$.

In simulations A, C, and D, we have initialised a right-hand polarized wave on the Alfvén wave branch of the dispersion equation, which propagates from left to right in the simulation domain. The details of this wave polarization are given in Mottez (2008). In the initialisation, in accordance with the linear theory, there is no parallel electric field associated to this wave. The wave amplitude is controlled through the intensity of the sinusoidal perpendicular magnetic field δB . There is one wavelength in the box.

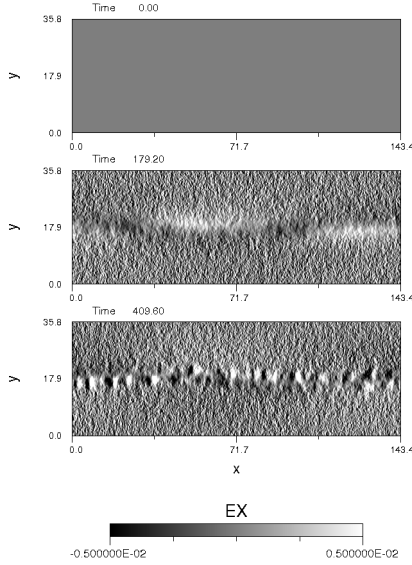


Fig. 4 Run D: snapshots from $t = 0$ to $t = 409.6$ of the parallel component of electric field $E_x(x, y)$.

The ratio of the wave frequency ω to ion cyclotron frequency is $\omega/\omega_{ci} \approx 1.317$ for $V_{Te} = 0.07$ (runs A and C); we are clearly not simulating a purely MHD Alfvén wave (it should correspond to $\omega/\omega_{ci} \ll 1$). We rather simulate an electron cyclotron wave, that is actually on the upper frequency part of the same dispersion relation branch as the MHD Alfvén wave. For $V_{Te} = 0.14$ (runs B and D), the ratio $\omega/\omega_{ci} \approx 0.54$. In all cases, our simulations relate to the high frequency part of the turbulent cascade of Alfvén waves, near the ion-cyclotron cut-off of the wave energy spectrum.

Nevertheless, in the paper, we speak of “Alfvén waves”, even if we must keep in mind that we actually simulate a wave on the higher frequency part of the dispersion relation branch related to them.

Run C corresponds to a simulation with a cavity of moderate amplitude ($p = 0.75$), and runs B, D to a simulation with a very deep amplitude ($p = 1$) and a less intense incident wave.

In what follows, we focus mainly on electric field and on the velocity distribution of electrons.

3 Electric fields

Run A is a test of Alfvén wave propagation through a uniform plasma ($p = 0$). Figure 1 shows the parallel electric field $E_x(x, y)$ from $t = 0$ to $t = 409.6$ for the run A. During this propagation, no parallel electric field and no compression of the plasma is observed in Figure 1 in spite of

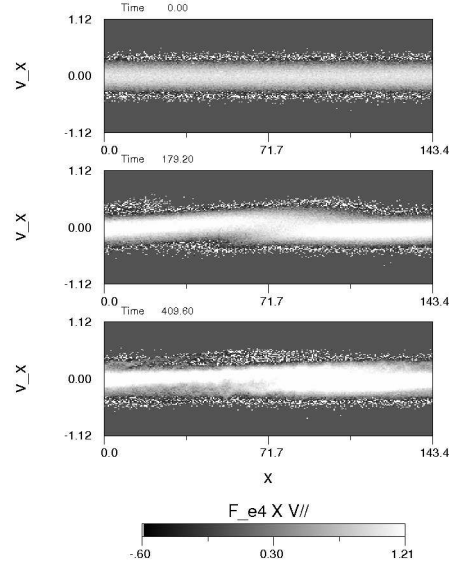


Fig. 5 Run D: snapshots from $t = 0$ to $t = 409.6$ of the electron distribution function $f_e(x, V_x)$ in logarithmic scale, at a fixed y (Figure 4).

quite large amplitude wave. Furthermore, the wave packet is not attenuated during the simulation and the wave vector remains parallel to the ambient magnetic field ($k_{\perp} = 0$).

Opposite to the run A, the plasma in run B is inhomogeneous with the presence of an interplume as a density cavity centred at $L_y/2$. However, no wave is set in the initial conditions. Figure 2 shows the component E_x displayed in the $x - y$ plane. The snapshots are from $t = 0$ to $t = 409.6$. No parallel electric fields were observed during all the simulations. Nevertheless, small electrostatic oscillations were observed for the E_y component in the transverse direction.

In runs B, C, D, we assume a pressure equilibrium condition for the cavity, as is the case of tangential discontinuities, which requires that the pressure inside the cavity is equal the pressure outside it. This condition implies a “correction” of the parallel background magnetic field as

$$B_x = B_0 \left[1 + \frac{\beta_0}{2} \left(1 - \frac{n}{n_0} \right) \right]. \quad (3)$$

Furthermore, to insure an MHD stability of the channel, we assume that the density gradient scale is large in comparison with ion gyroradius for all simulations. However, to construct a more stabilized tangential discontinuity, we need to apply plasma kinetic equations with non trivial electron velocity distribution. This could allow sharp cavities that are authentic equilibrium solutions without electric field (Channell 1976; Mottez 2004; Sitnov et al. 2006; Liu, Liang & Donovan 2010; Kocharovsky, Kocharovsky & Martyanov

2010), some of them being directly applied to plasma cavities (Mottez 2003). More recent computations show that sharp density gradients can also be associated to finite non-oscillating perpendicular electric fields (De Keyser, Echim & Roth 2013).

Run C includes an interplume and an Alfvén wave. We note at first that the cavity is not destroyed by the Alfvén wave (not shown on a figure). In Figure 3, the parallel electric field $E_x(x, y)$ and the parallel current density associated to the electrons $J_x(x, y)$ are represented through three different times. At time 179, a significant parallel electric field is clearly visible on the edges of the cavity. Along the x axis, the parallel electric field (E_x) structure has the same wavelength as the initial Alfvén wave. These characteristics are the same as those seen in the numerical simulations in Génot et al. (2004) made in the context of the Earth auroral zone, and in Tsiklauri et al. (2005) and Tsiklauri (2011) in the context of the solar corona.

As was shown previously (Génot, Louarn & Mottez 2000; Tsiklauri 2011), the wave velocity is higher in the low density regions than outside the cavities. A distortion of the wave front results from this velocity shifts, creating a situation similar to those of an oblique Alfvén wave (Génot, Louarn & Le Quéau 1999; Tsiklauri 2007). This effect is also known as "phase-mixing" (e.g., Heyvaerts & Priest 1983; Tsiklauri 2016a). As can be seen in Table 1, all the simulations are done in the inertial regime. The origin of the parallel electric field results from the bi-fluid theory of dispersive inertial Alfvén waves (Goertz 1984), that is relevant when $(m_i/m_e)\beta \ll 1$. In this context, two different opinions explain the origine of the parallel electric field E_{\parallel} and its dependance on the mass ratio m_i/m_e . Génot, Louarn & Le Quéau (1999) suggest that with an oblique Alfvén wave, the polarization drift moves the ions in the transverse direction creating a space charge on the density gradient regions. A charge density is created, as well as the parallel electric field, and neutrality can only be restored by the longitudinal motion of electrons. Then E_{\parallel} is proportional to the ion mass m_i as the polarization drift equation. The second suggestion by Tsiklauri (2007) consider that the cause of E_{\parallel} generation is electron and ion flow separation induced by the transverse density inhomogeneity, which is different from the electrostatic effect of charge separation. The author derive an analytic equation which explains the process of E_{\parallel} generation by ion-cyclotron waves. However, the obtained E_{\parallel} in this case decreases linearly as the inverse of m_i/m_e , i.e., proportional to $1/m_i$.

Overall, phase-mixing in the transversely inhomogeneous plasma naturally creates k_{\perp} , which in turn leads to E_{\parallel} .

In simulation C, we have calculated the maximum separation $(\Delta y)_{max}$ between ions and electrons on the density gradient (see Génot et al. 2004 for calculations). This value $\sim 11\lambda_{De}$ is an estimate of the width of the acceleration region in the transverse direction ($\lambda_{De} = 0.07$).

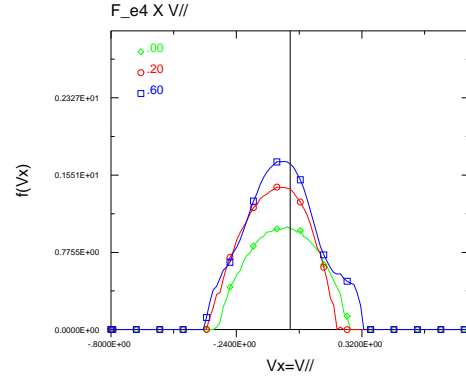


Fig. 6 Run D: a cut at $x = 72$ of the electron distribution function $f_e(x, V_x)$ as a function of the parallel velocity V_x . The three color curves are for different values of y .

4 Electron acceleration

Figure 4 shows the parallel electric field $E_x(x, y)$ for run D.

Figure 5 shows the electron distribution function $f_e(x, V_x)$ for $N_y/2 < y < 5N_y/8$, in logarithmic scale for Run D. In the snapshots at $t = 179.2$ and $t = 409.6$, we can distinguish clearly a beam of fast electrons escaping with velocities V_x about $3 V_{Te}$, which are larger than the incoming wave phase velocity ($V_A = 0.0315$). Therefore, a part of the accelerated electrons propagate temporarily in the front of the wave packet with a suprathermal velocity. In the case of Earth magnetosphere where the magnetic field is much higher, Mottez & Génot (2011) found the same result but with a much higher velocity for the electrons beam ($8V_{Te}$). In the snapshot at $t = 409.6$, the signature of instability is clearly seen in the form of a vortex structures associated to the electron beam. The electron holes associated to vortex structures trap the particles in their electric field and reduce the acceleration process.

Figure 6 shows a cut at $x = 72$ ($N_x = 512$) of the electron velocity distribution function for three different values of y . For the distribution function $y = 0.6$ (blue curve), a second small peak is visible at $V_x \sim 0.26 \approx 2V_{Te}$ which corresponds to the accelerated beam electrons.

This figure shows also a global shift of the distribution function in the parallel direction, particularly for the red and the blue curves. This indicates that electrons gained energy from their interaction with the parallel electric field in gradient regions of the cavity. The velocity drift is $V_{drift} \approx -0.06$, which is smaller than the thermal velocity. This explain also why we do not observe a Buneman instability.

5 Electron beam plasma instability

In run C, the typical size of the electric structure is those of the incident Alfvén wave ($\lambda = 71.7$). In run D (Figure 4), we observe smaller-scale bipolar electrostatic structures along the interplume cavity. Their typical scale is about 30 to $45\lambda_{De}$ which is twice or three times smaller than the struc-

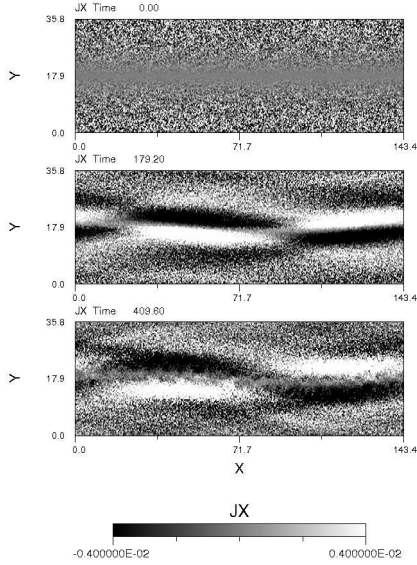


Fig. 7 Run D: snapshots from $t = 0$ to $t = 409.6$ of the parallel current density associated to the electrons $J_x(x, y)$.

tures found by Génot et al. (2004) in the context of the Earth auroral zone.

Figure 7 shows the parallel current density associated to the electrons. The signature of a strong acceleration of electrons in the interplume cavity is clearly apparent from $t = 0$ to $t = 179.2$. However, at $t = 409.6$, small transverse structures are visible.

Figure 8 shows the temporal evolution of the parallel electric field in Run D as a function of x , at $y = 16.8$ which is approximately the position of the small structures observed in the lower part of the interplume cavity (Figure 4). For $t < 200$, we can observe the evolution of the large scale parallel electric of the same size as the wavelength ($\lambda = 143.4$). These fields propagate from left to right sides as well as the Alfvén wave propagates. After $t \sim 250$, the large scale electric field disappears behind small bipolar structures of stronger amplitude. We can infer that these structures observed also in Figures 4 and 7 are a consequence of the non-linear evolution of an electron beam plasma instability. The accelerated electrons escape from acceleration regions and create a beam which interacts with the plasma. The beam becomes unstable causing a re-organization of the parallel electric field into small-scale quasi-linear structures. After $t \sim 307$, these structures are accelerated into the right hand side direction for $x > 15$, and they are accelerated into the left hand side direction for $x < 15$. For $t > 341$, we can also observe very weak structures between $x = 90$ and $x = 108$ that propagates only in the right hand side direction (positive slopes).

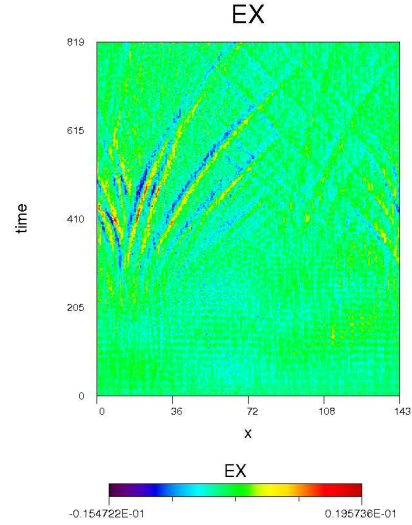


Fig. 8 Run D: the temporal variation of the component E_x of the wave as a function of the coordinate x and time at $y = 16.8$ ($N_y = 120$).

We have measured the velocity of these structures by measuring the positive and negative slopes of the observed stripes:

For the largest slope, we have found $V_x = 0.07 \approx V_{Te}/2$ in left and $V_x = 0.21 \approx 1.5V_{Te}$ in right. These last values are in accordance with the velocity measured in Figure 6 for the beam propagating in the right hand side direction.

For the smallest positive slopes, we have found $V_x \approx 0.033$ for the stripes at $x = 15$, and $V_x \approx 0.0286$ for the weak stripes situated between $x = 90$ and $x = 108$ ($t > 334$). This shows that another part of the electron population propagates around the phase velocity of the Alfvén wave ($V_A = 0.0315$), which indicates a signature of Landau damping due to the wave-particle interaction (see for example Tsiklauri 2016b).

We can notice that the small scale structures present analogies with the coherent structures observed in the Earth auroral zone acceleration regions (Temerin 1982; Mottez et al. 1997; Ergun et al. 1998). Isolated bipolar electrostatic structures in the solar atmosphere and particularly in the solar wind were analysed in Mangeney et al. (1999) with the *WIND/WAVES* waveform analyser. It was found that these structures are isolated spikes of duration 0.3 to 1 millisecond. They consist of two main weak layers of approximately opposite charge with a spatial width $\sim 25\lambda_{De}$ close to the thickness of the structures observed in our simulation. Compared to the Earth magnetosphere environment, it seems that the background magnetic field strength is related

to the size of these structures. The observations show also that these structures propagate along the magnetic field line at a velocity smaller than the solar wind velocity. However, the double layers in the solar wind are seen in a uniform plasma, while those that we have simulated are seen in the environment of a deep cavity.

We have to note that the limitation in the non-linear interactions in the space (2D) might favour the transfer of energy to parallel fluctuations, since the perpendicular direction is absent. In a more realistic 3D scenario, the conversion to the perpendicular electric field would be much more pronounced, reducing the acceleration effect in the parallel direction.

6 Conclusion

The detection of suprathermal electrons in the solar atmosphere remains a current problem. Different acceleration processes based on magnetic reconnection have been proposed. However, observations indicate that electrons are accelerated even in the absence of solar flares. In this paper, we have presented 2.5 D particle-in-cell numerical simulations of Alfvén wave propagation through an interplume region. The interplume structure is modeled by a cavity density gradient perpendicular to the background magnetic field. We have started the simulations with conditions similar to those of the solar coronal holes. The aim is to contribute to the explanation of the observation of high energy electrons in solar corona through wave-particle interactions.

We have showed that an Alfvén wave propagating along a typical interplume in inertial regime is able to generate electric fields parallel to the ambient magnetic field in the solar radial direction. The electric fields are localised in the density gradient regions with a typical size about the wavelength of the Alfvén wave. These electric fields can accelerate and heat electrons in the parallel direction.

In the case of strong amplitude cavity and less intense Alfvén wave, we have found that accelerated electrons can reach velocities about $2V_{Te}$. They form beams and they generate a beam plasma instability whose non-linear evolution results in small scale electrostatic structures.

These features can be identified as weak double layers. They present similarities with the spikes observed in the solar wind with *WIND/WAVES* waveform analyser. We note that despite the strong amplitude of the Alfvén wave propagating along it, the cavity is not destroyed. This indicates that interplumes are stable structures that could survive during the Alfvén waves propagation.

Modeling the acceleration source in interplume regions is a real challenge regarding the lack of high spatial resolution by solar observatories. In our simulation, the largest transversal width of the interplume cavity is of order of $256 \lambda_D$, which corresponds to 388 m. The today highest spatial resolution measured with *TRACE* is about 370 km, which makes the observation of such small scale structures impossible. However, many characteristics of interplume struc-

tures remain poorly understood like their cross-sections and their life. Possibility of fractal nature of plumes was invoked by some authors (e.g., Llebaria et al. 2002; Milovanov & Zelenyi 1994; Boursier & Llebaria 2008), which implies the possibility of existence of interplume microstructures. The future high spatial resolution measurements by Solar Probe Plus and Solar Orbiter space missions may resolve these fine structures, and provide further details about the heating and the acceleration of particles in interplume regions.

Acknowledgements. The authors thank the anonymous referee for constructive comments and suggestions that improve the quality of the paper.

References

- Bale, S. D., Kellogg, P. J., Mozer, F. S., Horbury, T. S., & Reme, H. 2005, *Phys. Rev. Lett.*, 94, 215002
- Banerjee, D., Gupta, G. R., & Teriaca, L. 2011, *Space Sci. Rev.*, 158, 267
- Biskamp, D., Schwarz, E., Zeiler, A., Celani, A., & Drake, J. F. 1999, *Phys. Plasmas*, 6, 751
- Boursier, Y., & Llebaria, A. 2008, *Statistical Methodology*, 5, 328
- Carlson, C. W., McFadden, J. P., Ergun, R. E., et al. 1998, *Geophys. Res. Lett.*, 25, 2017
- Channell, P. J. 1976, *Phys. Fluids*, 19, 1541
- Cranmer, S. R. 2009, *Living Reviews in Solar Physics*, 6, 3
- De Keyser, J., Echim, M., & Roth, M. 2013, *Ann. Geophysicae*, 31, 1297
- Ergun, R. E., Carlson, C. W., McFadden, J. P., et al. 1998, *Geophys. Res. Lett.*, 25, 2025
- Génot, V., Louarn, P., & Le Quéau, D. 1999, *J. Geophys. Res.*, 104, 22649
- Génot, V., Louarn, P., & Mottez, F. 2000, *J. Geophys. Res.*, 105, 27611
- Génot, V., Louarn, P., & Mottez, F. 2004, *Ann. Geophysicae*, 22, 2001
- Génot, V., Mottez, F., & Louarn, P. 2001, *Phys. Chem. Earth C*, 26, 219
- Goertz, C. K. 1984, *Planet. Space Sci.*, 32, 1387
- Goldstein, M. L. & Roberts, D. A. 1999, *Phys. Plasmas*, 6, 4154
- Gupta, G. R., Banerjee, D., Teriaca, L., Imada, S., & Solanki, S. 2010, *ApJ*, 718, 11
- Heyvaerts, J., & Priest, E. R. 1983, *A&A*, 117, 220
- Hilgers, A., Holback, B., Holmgren, G., & Bostrom, R. 1992, *J. Geophys. Res.*, 97, 8631
- Ito, H., Tsuneta, S., Shiota, D., Tokumaru, M., & Fujiki, K. 2010, *ApJ*, 719, 131
- Kocharovskiy, V. V., Kocharovskiy, V. V., & Martyanov, V. J. 2010, *Phys. Rev. Lett.*, 104, 215002
- Lin, R. P. 1980, *Sol. Phys.*, 67, 393
- Liu, W. W., Liang, J., & Donovan, E. F. 2010, *J. Geophys. Res. (Space Phys.)*, 115, A03211
- Llebaria, A., Saez, F., & Lamy, P. 2002, *From Solar Min to Max: Half a Solar Cycle with SOHO*, 508, 391
- Louarn, P., Wahlund, J. E., Chust, T., et al. 1994, *Geophys. Res. Lett.*, 21, 1847
- Mangeney, A., Salem, C., Lacombe, C., et al. 1999, *Ann. Geophysicae*, 17, 307
- McIntosh, S. W., de Pontieu, B., Carlsson, M., et al. 2011, *Nature*, 475, 477

- Milovanov, A. V., & Zelenyi, L. M. 1994, Washington DC American Geophysical Union Geophysical Monograph Series, 84, 43
- Mottez, F. 2003, Phys. Plasmas, 10, 2501
- Mottez, F. 2004, Ann. Geophysicae, 22, 3033
- Mottez, F. 2008, J. Comput. Phys., 227, 3260
- Mottez, F. & Génot, V. 2011, J. Geophys. Res.(Space Phys.), 116, A00K15
- Mottez, F., Adam, J. C., & Heron, A. 1998, Computer Phys. Communications, 113, 109
- Mottez, F., Perraut, S., Roux, A., & Louarn, P. 1997, J. Geophys. Res., 102, 11399
- Newkirk, G. Jr., & Harvey, J. 1968, Sol. Phys., 3, 321
- Ofman, L. 2005, Space Sci. Rev., 120, 67
- Pierrard, V., Maksimovic, M., & Lemaire, J. 1999, J. Geophys. Res., 104, 17021
- Podesta, J. J. & TenBarge J. M. 2012, J. Geophys. Res.(Space Phys.), 117, A10106
- Poletto, G. 2015, Living Reviews in Solar Physics, 12, 7
- Sahraoui, F., Huang, S. Y., Belmont, G., et al. 2013, ApJ, 777, 15
- Sitnov, M. I., Swisdak, M., Guzdar, P. N., & Runov, A. 2006, J. Geophys. Res.(Space Phys.), 111, A08204
- Temerin, M., Cerny, K., Lotko, W., & Mozer F. S. 1982, Phys. Rev. Lett., 48, 1175
- Thurgood, J. O., Morton, R. J., & McLaughlin, J. A. 2014, ApJ, 790, L2
- Tsiklauri, D. 2007, New J. Phys, 9, 262
- Tsiklauri, D. 2011, Phys. Plasmas, 18, 092903
- Tsiklauri, D. 2012, Phys. Plasmas, 19, 082903
- Tsiklauri, D. 2016a, A&A, 586, A95
- Tsiklauri, D. 2016b, Phys. Plasmas, 23, 122906
- Tsiklauri, D., Sakai, J.-L., & Saito, S. 2005, A&A, 435, 1105
- Tsuneta, S., Ichimoto, K., Katsukawa, Y., et al. 2008, ApJ, 688, 1374-1381
- Wilhelm, K., Marsch, E., Dwivedi, B. N., et al. 1998, ApJ, 500, 1023
- Wilhelm, K. 2006, A&A, 455, 697
- Wilhelm, K., Abbo, L., Auchère, F., et al. 2011, A&A Rev., 19, 35
- Wu, D. J., & Fang, C. 2003, ApJ, 596, 656
- Zhao, J. S., Wu, D. J., & Lu, J. Y. 2013, ApJ, 767, 109